Solid Particle Number and Mass Emissions from Lean and Stoichiometric Gasoline Direct Injection Engine Operation

Abstract

In this work, engine-out particle mass (PM) and particle number (PN) emissions were experimentally examined from a gasoline direct injection (GDI) engine operating in two lean combustion modes and one stoichiometric mode with a fuel of known properties. Ten steady state operating points, two constant speed load steps, and an engine cold start were examined. Results showed that solid particles emitted from the engine under steady state stoichiometric conditions had a uniquely broad size distribution that was relatively flat between the diameters of 10 and 100 nm. In most operating conditions, lean homogenous modes can achieve lower particle emissions than stoichiometric modes while improving engine thermal efficiency. Alternatively, lean stratified operating modes resulted in significantly higher PN and PM emissions than both lean homogeneous and stoichiometric modes with increased efficiency only at low engine load. Stoichiometric load steps showed minimal soot emissions while ash-mode emissions spike dramatically due to oil consumption caused by piston ring adjustment. Correlation of PN to PM for steady state stoichiometric cases was in good agreement with that reported from multiple prior studies for both diesel and stoichiometric GDI engines. However, the lean cases resulted in higher PN to PM ratios indicating more small particles per unit mass. High ash particle concentration, especially in lean operation illustrates that oil control is important for mitigating impacts on downstream gasoline particulate filters (GPF) from which ash particles are cannot be removed during filter regeneration. Further research is necessary to elucidate the origin and composition of sub-23 nm particles from GDI engines and their effect on aftertreatment technology if lean homogeneous modes are to be employed.

Introduction

Continued pressure exists to improve vehicle fuel economy to meet corporate average fuel economy (CAFE) standards. Many vehicle manufacturers are meeting this challenge by implementing gasoline direct injection GDI engines which offer increased fuel economy over their port fuel injection (PFI) counterparts. GDI engines can improve fuel economy through greater charge cooling, more precise fuel metering, and by allowing higher compression ratios [1]. GDI engines also enable the possibility of lean operation which further increases engine efficiency by reducing throttling losses and increasing the specific heat ratio of the charge. However, GDI engines are plagued by high particulate matter emissions compared to PFI engines [2–7] and modern diesel engines employing diesel particulate filters (DPF) [8–10]. The high PM/PN associated with GDI engines is generally a result of local rich zones associated with poor charge mixture and/or fuel impingement on cylinder surfaces [11]. Significant fuel stratification is required to achieve very low equivalence ratios, which inherently increases charge inhomogeneity leading to higher particulate emissions.

Further complicating the introduction of lean GDI engines, particle emissions regulations are becoming increasingly stringent. Specifically, the California Air Resources Board (CARB) LEV III PM emissions standards are an upcoming challenge for GDI engines as the 3 mg/mi limit is currently being phased in and a 1 mg/mi limit will be phased in starting in 2025 [12]. Additionally, the European Commission enacted the first limit on PN from GDI vehicles of $6x10^{12}$ solid particles > 23 nm per km with the Euro 6 standard from 2014. The limit was reduced to $6x10^{11}$ solid particles > 23 nm per km in 2017 [13].

Non-volatile sub-23nm particles composed of non-soluble metal oxides thought to originate from fuel and/or lube oil additives have been shown to make up a substantial portion of GDI PN[14–16] and can dominate solid particle number (SPN) distributions measured from PFI engines [17]. Typically, engines emit total PN size distributions that fit a bimodal lognormal distribution comprising a mainly semi-volatile nucleation mode and a carbonaceous accumulation mode [18]. The soot mode usually scavenges most of the semi-volatile material as well as metallic ash formed from metals in the lube oil. However, when little soot is present, a separate, solid ash mode may be formed in the 10 nm range. When semi-volatile material is removed prior to measurement, this “ash-mode” remains. This 10 nm ash mode is not counted in current emissions standards because it only accounts for a tiny fraction of PM that would be measured under the CARB LEV III regulation and is below the 23 nm threshold for PN under current EU rules. However, smaller particles pose greater toxicological harm due to increased surface to volume ratio, higher penetration into the human respiratory system, and increased likelihood of passage through cell membranes and the blood brain barrier [19,20]. For these reasons, future PN regulations could include particles as small as 10 nm. It is likely that this regulation could only be met by implementing GPFs.

It has been shown GDI engine cold starts and accelerations dominate PN/PM emissions during various drive cycles [21–23]. Diesel and spark ignition engines both have been shown to have high ash mode emissions during cold start and idle like conditions [24]. A thorough review of the literature conducted in 2014 showed the percentage of sub-23 nm SPN is typically between 30-40% for stoichiometric GDI engines [25]. The objective of this study is to characterize particle emissions from lean and stoichiometric GDI engines operating in representative steady state and transient conditions. This body of work will become a baseline to which various combustion strategies, fuel properties and aftertreatment technologies can be compared for mitigating particle emissions from GDI engines.

Experimental

A BMW N43B20, four-cylinder, 2.0 L, naturally aspirated engine with centrally mounted spray guided piezo injectors was used for this study. The engine operated in three combustion modes: stoichiometric, lean homogeneous, and lean stratified. Table 1 details relevant engine specifications. Full control of all engine parameters was enabled by National Instruments (NI) software and hardware in lieu of the factory engine control unit (ECU). The software calibration was developed by another research group with the factory ECU and the vehicle on a chassis dynamometer to closely match the engine modes employed by the factory ECU.

Table 1. Engine specifications

Model Number	N43B20
Displacement (cc)	1995
Bore x Stroke (mm)	84 x 90
Compression Ratio	12:1
Rated Power (kW)	125 @ 6700 rpm
Rated Torque (Nm)	210 @ 4250
Induction	Naturally Aspirated
Injection	Central Spray Guided Piezo Injectors
Max Rail Pressure (bar)	200

The three engine combustion modes differed in equivalence ratio and injection strategy. The stoichiometric operating mode featured fuel injection during the intake stroke. The lean homogeneous mode used a partially stratified charge injection strategy to operate with a globally lean equivalence ratio. This was accomplished by injecting most of the fuel during the intake stroke to achieve a lean homogenous charge mixture with a subsequent injection during the compression stroke, resulting in a partially stratified charge near the spark plug. Equivalence ratios as low as ~ 0.65 were achievable for this mode. The factory engine calibration used the lean homogeneous mode for moderate load speed and load conditions. The lean stratified operating mode featured two injections in rapid succession during the compression just prior to the spark event followed by a third injection immediately after the spark event. Lower equivalence ratios (< 0.5) are attainable with this injection strategy but it was limited to low speed, low load operating conditions. Rail pressure was maintained at 155 bar for all conditions.

Ten steady state operating conditions and three transient operating conditions were evaluated in this study and are shown in Table 2 with corresponding equivalence ratio. The steady state operating conditions included stoichiometric, lean homogeneous, and lean stratified operating modes. The transients included two constant speed load steps at 2000 rpm from 2 bar to 7 bar brake mean effective pressure (BMEP) in stoichiometric and lean homogeneous and a stoichiometric cold start at 1000 rpm.

It has been shown that injector deposit formation has a strong impact on PN and PM emissions from GDI engines [26]. Fuel adsorption on the injector deposit results in diffusion flames; a known cause of particle emissions in GDI engines. Running the engine at high speed and high load can effectively burn off deposits and return the emissions to that from an engine with clean injectors. To attain repeatable particle emissions at a given condition from test to test, each condition in the test matrix was run in the same specific order with the same amount of time (to the second) spent at each condition. This was implemented by an automated test plan during which all controllable engine and dynamometer parameters were compiled in spreadsheet with a specified time step for each condition. The data was then fed to a program that wrote the parameters to the engine and dynamometer controllers. A high speed/high load “de-coking” condition (2500 rpm 8 bar BMEP) preceded each set of engine mode operations (i.e., a high speed/high load condition before stoichiometric operation, a high speed/high load condition before lean homogeneous operation etc.) to burn off injector deposits and set a baseline engine state to proceed from.

The complete test matrix was performed once per day for a total of three tests conducted on three separate days. Two minute averages of all measured parameters were taken at the same temporal period in each test such that level of injector deposit formation was assumed to be the same for a given condition from test to test. For the steady state conditions, this measurement period was from 12 min to 14 min elapsed at the given condition. This was more than sufficient time for exhaust and in-cylinder temperatures to stabilize, however not necessarily for PN/PM emissions to stabilize as injector coking evolution may be on the order of hours [27].

Table 2. Engine conditions including operating mode and equivalence ratio. S = stoichiometric, LH = lean homogeneous, and LS = lean stratified.

Condition	Speed (rpm)	BMEP (bar)	Mode	φ
SS 1	1400	2	S	1.0
	1400	2	LH	0.67
	1400	2	LS	0.5
SS 2	2000	4	S	1.0
	2000	4	LH	0.65
	2000	4	LS	0.65
SS 3	2000	7	S	1.0
	2000	7	LH	0.69
SS 4	2400	7	S	1.0
	2400	7	LH	0.73
Load steps	2000	2-7	S	1.0
	2000	2-7	LH	0.73 – 0.67
Engine start	1000	0	S	1.0

Constant speed load steps were conducted by sweeping all engine parameters from the calibration point at 2 bar BMEP to the calibration point at 7 bar BMEP by linear interpolation at a rate of 10 steps per second over a period of 3 seconds. This was done by creating a table of engine parameters (i.e. injection timing, spark timing, MAP, cam phasing etc.) with a resolution of 0.1 seconds through which the engine controller stepped when commanded. The motivation was to attain greater repeatability than having the engine controller utilize maps (look-up tables) for changing engine parameters when an increased throttle position was detected. Fuel quantity was controlled by closed loop lambda control on each cylinder. The engine cold start was conducted by motoring the engine at 1000 rpm for 30 seconds, setting a predetermined manifold absolute pressure (MAP) value, letting rail pressure reach 15.5 MPa, and then enabling spark and injection. This procedure was started after the engine controller synchronized the cam and crank angle sensors. The air/fuel ratio was controlled by the mass air flow (MAF) sensor until the wide band oxygen sensors reach operating temperature after which closed loop control proceeded. The cold start was conducted at a stoichiometric air/fuel ratio, i.e. with no fuel enrichment. Although this procedure did not precisely mimic the cold start in an actual vehicle, it was repeatable and represented a suitable baseline to which different strategies could be compared.

An oxygenated 90.8 anti-knock index (AKI) fuel containing no additives was used for all testing. The fuel composition included 27% aromatics and 9.94% ethanol with properties including a T90 distillation temperature of 161.6 °C and a research and motor octane number of 96.2 and 85.4 respectively.

Gaseous emissions were measured by an AVL (Graz, Austria) SESAM i60 multi-component exhaust measurement system composed of a Fourier transform infrared spectrometer (FTIR) for

gas phase speciation, a flame ionization detector (FID) for measuring unburned hydrocarbon concentrations, and separate CO_2 non-dispersive infrared (NDIR) analyzer. Particle measurements included an AVL Micro Soot Sensor (MSS) for measuring soot mass concentration, a TSI (Shoreview, MN) engine exhaust particle sizer (EEPS) spectrometer with the soot inversion matrix for measuring particle size distributions (PSD) at a rate of 1 Hz, and a TSI scanning mobility particle sizer (SMPS) spectrometer for measuring PSDs. It should be noted that the MSS measures light absorbing carbon, or black carbon and is calibrated against elemental carbon. SMPS measurements were taken at steady state conditions with a scan time of 60 seconds to verify size distributions measured by the EEPS.

Figure 1 shows the exhaust sampling system and instrumentation used in the study. Dilution was achieved using ejector pump (EP) diluters with critical orifices upstream of the sample flow. The primary dilution ratio was calculated throughout testing on a second by second basis by the ratio of the undiluted to primary diluted CO_2 concentrations as the dilution air was free of CO_2. The primary dilution ratio was approximately 12:1 and the secondary dilution ratio was 40:1. Secondary dilution was used to keep particle concentrations within ranges required by the EEPS and SMPS for engine conditions with high PN concentrations. The critical orifices upstream of the ejector pumps were used to maintain a constant volumetric flow rate (choked flow) of the sample flow. The mass flow rate of the primary sample flow varied slightly corresponding to fluctuations in density of the exhaust stream caused by changes in exhaust temperature and pressure. The conditions upstream of the secondary dilution ejector pump were constant, thus the dilution ratio was assumed to be constant throughout the test and was only measured prior to each test. A catalytic stripper (CS) operated at 300 °C was used upstream of the EEPS and SMPS to remove all volatile and semi-volatile material such that the particle size distributions measured were that of only solid particles. The design and performance of the CS is discussed at length in other work [28].

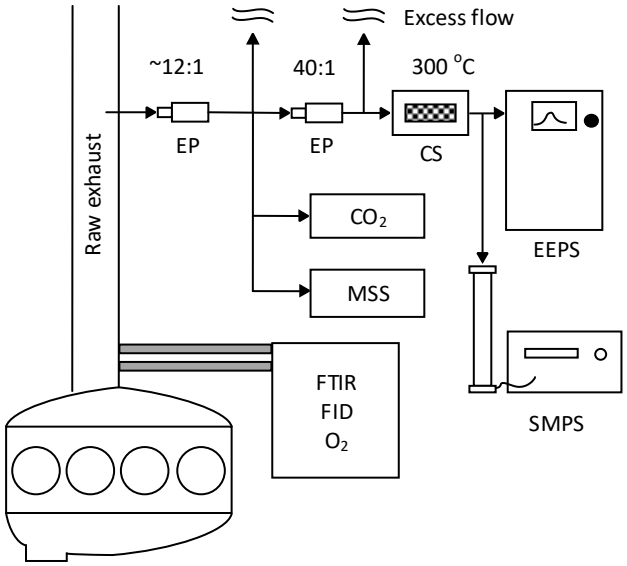

Figure 1. Engine and instrumentation schematic showing dilution system and instruments used in the experimental study.

It has been shown that re-nucleation of semi-volatile material can occur downstream of the volatile particle removers (VPR) employed by particle measurement programme (PMP) sampling systems resulting in sub-23 nm particles [17]. This is not of concern when using a PMP protocol compliant system with a particle counter with a 23 nm cut-off size. However, because sub-23 nm particle emissions were of interest for this study, a CS was used instead of a VPR because the CS more effectively removes semi-volatile material [28,29].

Loss through the CS was characterized by challenging the CS with atomized NaCl particles of four different mobility diameters (15 nm 30 nm, 50 nm and 100 nm) classified by a differential mobility analyzer (DMA). The penetration of these particles was calculated by measured concentrations upstream and downstream of the CS using a condensation particle counter (CPC). A penetration model based on size dependent laminar diffusion losses and essentially size independent thermophoretic losses was fit to the measured penetration data. This penetration model was then applied to the EEPS and SMPS data to obtain size-resolved loss-corrected particle size distributions. The loss correction was significant, especially for small particles. It increased total solid number concentrations by 40 to 80 %.

Results and Discussion

Figure 2 shows the average brake specific fuel consumption (BSFC) for each of the steady state conditions. At the low speed/low load condition of 1400 rpm 2 bar BMEP, the lean stratified operating mode showed a significant fuel efficiency advantage over the lean homogeneous and stoichiometric operating modes which can be attributed to the lower equivalence ratio ($\varphi = 0.5$). Specifically, there was an 8.6% and 19% reduction in fuel consumption at this speed load condition compared to the lean homogenous and stoichiometric modes respectively, and an 11% reduction in fuel consumption from stoichiometric to lean homogeneous. At the 2000 rpm 4 bar BMEP condition, the fuel efficiency was approximately equal for the lean operating modes which show a marginal increase in fuel efficiency compared to the stoichiometric mode. Note from Table 2 that the lean operating modes shared the same equivalence ratio at this speed and load condition. There was a slight advantage for the lean homogeneous mode at this condition that can be attributed to the earlier combustion phasing of the lean stratified case in which MFB50 is at approximately top dead center as opposed to an ideal value for maximum brake torque of 7 CAD. The lean homogeneous 2400 rpm 7 bar condition had the lowest BSFC with 222 g/kWh corresponding to a brake thermal efficiency of 37.2% for E10 gasoline.

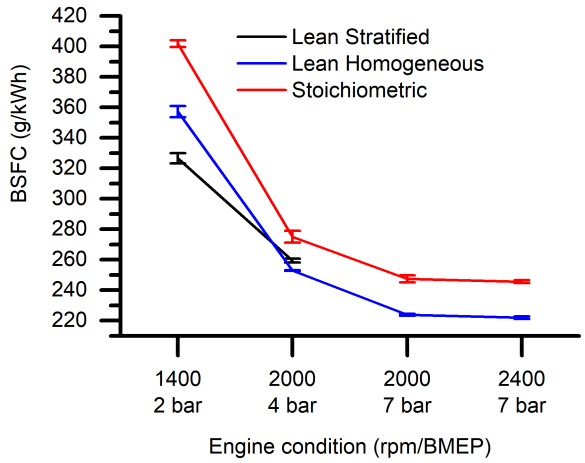

Figure 2. Average BSFC for the 10 steady state engine conditions. Error bars represent one standard deviation.

Figure 3 and Figure 4 show the brake specific SPN > 10 nm and brake specific soot concentrations for each of the steady state operating conditions respectively. The lean stratified operating modes emitted one to two orders of magnitude higher PN > 10 nm concentrations and two to three orders of magnitude higher soot concentration than the lean homogenous and stoichiometric modes at the respective conditions. The 2000 rpm 7 bar BMEP condition was the only case in which the lean homogeneous mode emits more SPN > 10 nm than the stoichiometric mode. Tailpipe exhaust concentrations for the two modes were approximately equal, but because the exhaust flow rate was higher for the lean homogeneous case, the brake specific emissions were higher. The stoichiometric mode produces higher soot emissions than the lean homogeneous mode for all conditions.

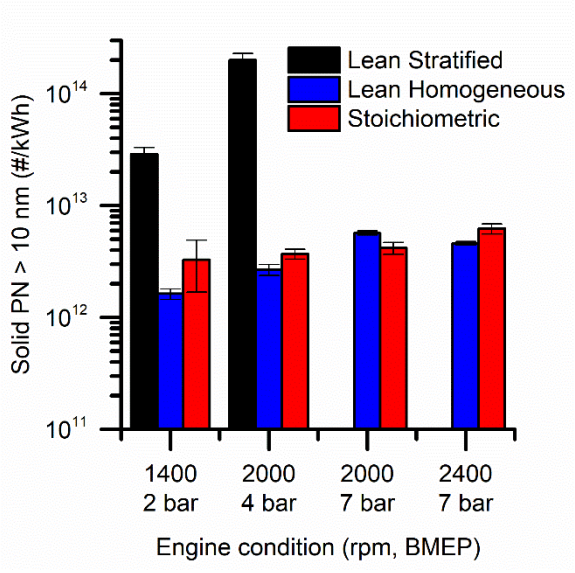

Figure 3. Average brake specific solid PN > 10 nm emissions as measured by EEPS for the 10 steady state engine conditions. Error bars represent one standard deviation.

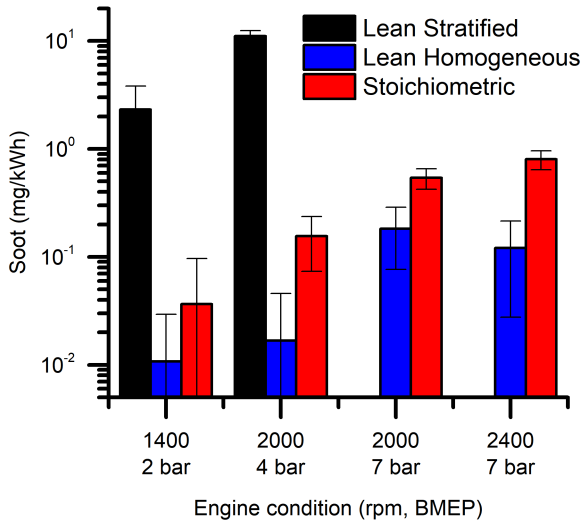

Figure 4. Average brake specific soot emissions as measured by MSS for the 10 steady state engine conditions. Error bars represent one standard deviation.

Figure 5 shows the fraction of solid PN > 10 nm that is between 10 and 23 nm for each steady state condition. The stoichiometric 4 and 7 bar BMEP conditions were on the high end of what is reported in the literature. However, all lean homogeneous cases are dominated by SPN between 10 and 23 nm. It is presumed that the particles in this size range are predominately composed of ash. This ash mode is likely highly sensitive to fuel and oil composition as well as engine oil consumption. The fraction of ash emitted in the nucleation mode range is also dependent upon the amount of soot present to scavenge ash. Thus the lean stratified condition with its large soot modes is associated with a smaller fraction of tiny ash particles. Future work will look to confirm composition of these particles using the methods described by Apple et al. 2009 [30].

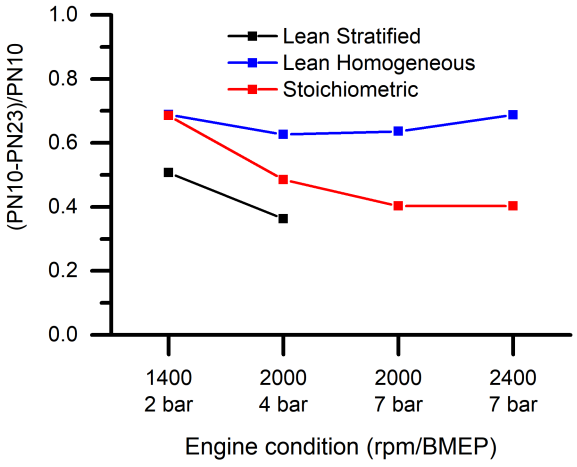

Figure 5. SPN > 10 nm fraction between 10 nm and 23 nm.

Figure 6 shows the average solid particle size distributions (PSD) for all the steady state conditions as measured using the EEPS instrument. As with all measurements taken for the steady state conditions, they are the average of three two-minute averages taken for each test with error bars showing the standard deviation between

the three test averages. Thus, the error bars represent the repeatability of the tests rather than the stability of the emissions during the sampling period. Large accumulation modes present for the lean stratified conditions are consistent with the high soot mass measured by the MSS. The lean homogeneous and stoichiometric operating modes had very similar ash modes at 10 nm except for the 1400 rpm 2 bar BMEP conditions which were slightly lower than the other cases but still dominate their respective size distributions.

Interestingly, the three higher speed and load stoichiometric conditions exhibited a very flat and broad PSD shape. The EEPS measurements were in good agreement with SMPS scans, not shown for brevity, taken at the same conditions. This flat distribution is not consistent with the well-recognized lognormal bimodal distributions traditionally associated with diesel and GDI engine combustion. This unusual feature may be characteristic of this engine model as Parks et al. reported similar size distributions from the same engine [31,32]. Ongoing work is aimed at understanding the formation mechanisms that underlie these results. The modal structure of diesel exhaust size distributions is associated with formation processes distinct in space and time. The soot mode is formed in a small number of rather well defined burning fuel jets. It may be that in the engine tested here, the temperature, composition histories of burning fuel packets are more heterogeneous, leading to a broader range of soot particle diameters.

Figure 7 shows the correlation between soot emissions measured by the MSS and PM emissions calculated from the EEPS volume measurement assuming a constant particle density of 0.7 g/cm^3. The results of a linear regression with the equation of the fit and R-squared value are shown for each mode. There is good agreement between the MSS and EEPS for the lean homogeneous modes. However, the MSS reported higher mass than the EEPS for all stoichiometric conditions, suggesting that the density estimate of 0.7 g/cc is too low for the stoichiometric conditions. This may be due to soot agglomerates with more compact structures for this mode. Conversely, the MSS reported lower mass than the EEPS for the lean stratified condition, suggesting that the density estimate was too high and that the soot particles from this mode are composed of more loosely packed core particles.

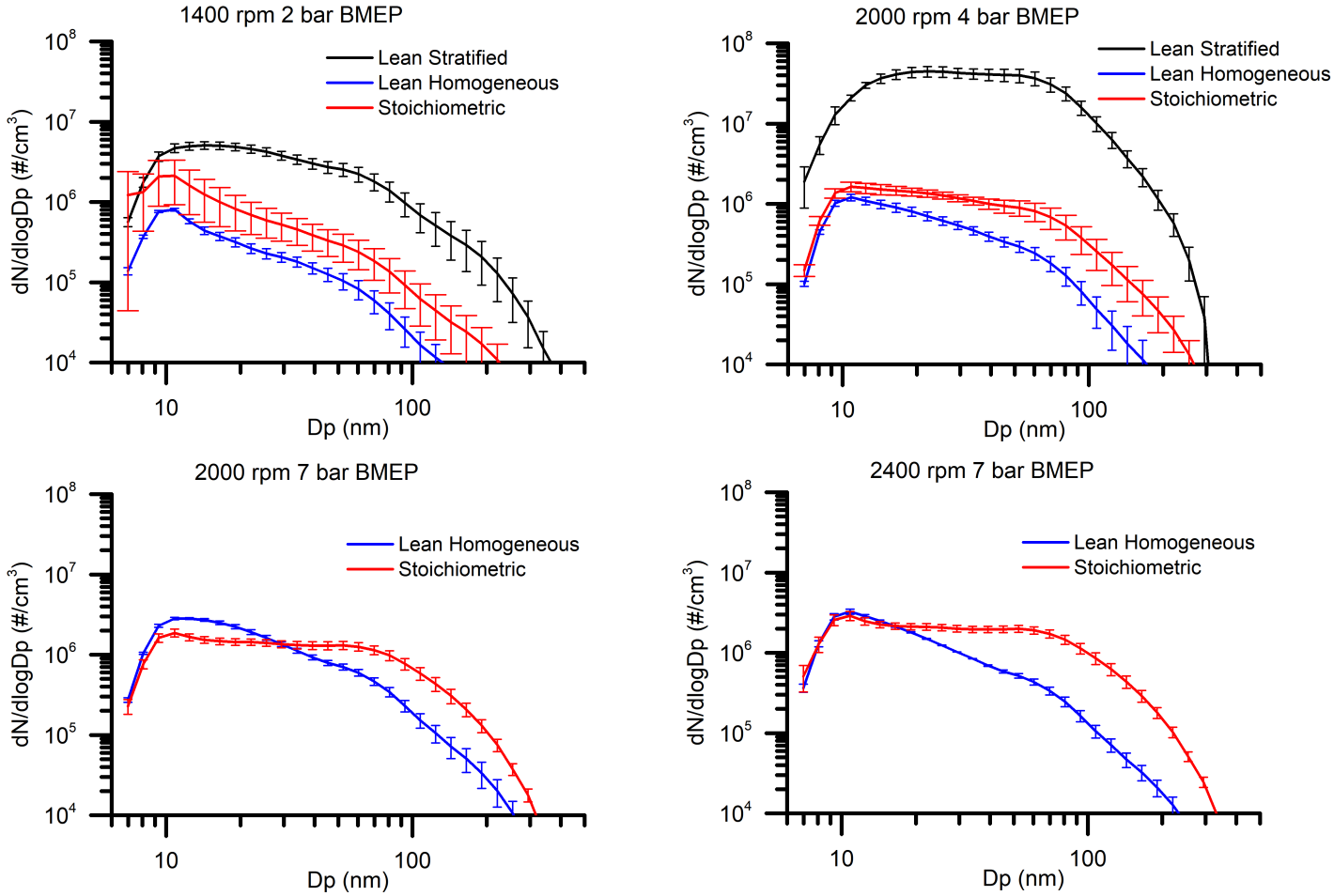

Figure 6. Particle size distributions measured by EEPS for each of the 10 steady state engine conditions. Error bars represent one standard deviation.

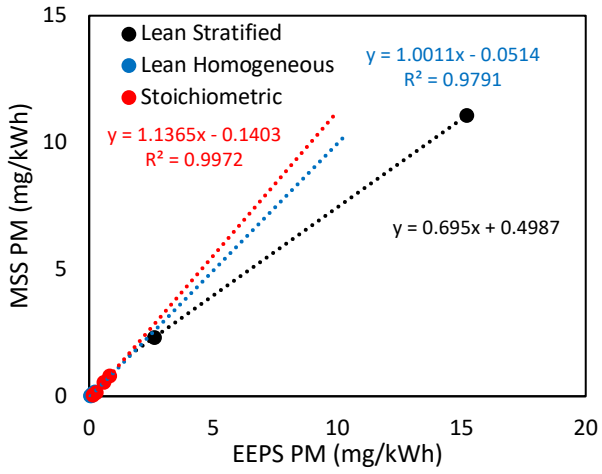

Figure 7. Correlation between MSS and PM calculated by EEPS.

Figure 8 shows the correlation between SPN and PM emissions calculated from the aerosol volume measured by the EEPS assuming constant particle density of 0.7 g/cm^3. Khalek et al. [21] reported a solid PN to PM ratio of 3.16 x 10^{12} with an R-squared value of 0.957 for a stoichiometric GDI engine using an EEPS with a catalytic stripper, the same method used in this study. This line is shown in Figure 8 for reference. The results of the current study show a similar PN to PM slope of 2.51 x 10^{12} #/mg for the stoichiometric mode though, the regression shows poor correlation with a linear fit. This can be attributed to the large ash mode of the 1400 rpm 2 bar BMEP condition. When SPN > 23 nm was plotted against PM measured by the EEPS, the slope was 3.30 x 10^{12} #/mg with an R-squared value of 0.970, which is very close to that reported by Khalek et al.

Although the steady state stoichiometric cases have PN to PM ratios similar to those found in literature for GDI engines, lean combustion modes exhibited much higher ratios than the stoichiometric combustion modes, indicating a higher number of small particles per unit mass. This is confirmed by examination of the lean homogeneous PSDs, which exhibit a prevalent ash mode followed by a steep drop in concentration as particle size increases, and by the plot in Figure 5 showing the lean homogeneous mode had the highest fraction of particles between 10 and 23 nm. For the lean stratified case, this result can also be observed in the PSD of the 2000 rpm 4 bar BMEP condition, although it is subtler. The PSD of this condition is very flat between 20 and 100 nm before dropping very sharply at higher particle sizes where most of the aerosol mass exists. Additionally, the lean stratified modes may produce particles of lower density as was mentioned previously. Due to the limited number of lean stratified operating points examined in this study, the number to mass correlation for this combustion mode is less than definitive. Effective density measurements from each mode to confirm this is of interest for future work.

Figure 9 shows the correlation of SPN > 23 nm and soot mass emissions measured by the MSS. Maricq et al. reported a PN to PM ratio of 2 x 10^{12} #/mg using a condensation particle counter (CPC) for PN measurement and a Dekati Mass Monitor for PM measurement [33]. This line is shown in Figure 9 for reference. When SPN > 23 nm was plotted against MSS PM, the slope was 3.09 x 10^{12} #/mg with an R-squared value of 0.939. Kirchner et al. reported a PN to PM ratio of 1.81 x 10^{12} #/mg for diesel exhaust particle emissions using an AVL APC489 for PN measurement and an MSS for soot mass measurement [34]. The stoichiometric number to mass ratio calculated using the EEPS and MSS is in good agreement with previous studies for PN > 23 nm, showing that the test engine has similar particle emissions characteristics to different GDI engines when the ash mode is neglected. However, it is apparent that lean combustion in the same engine results in more particles per unit mass than for stoichiometric modes.

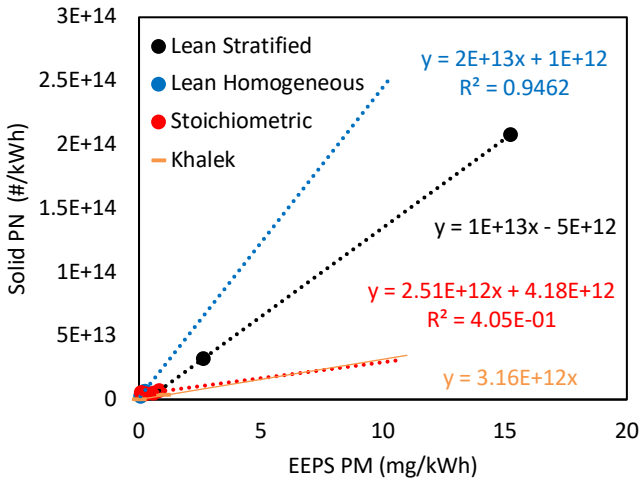

Figure 8. Correlation between SPN and PM calculated by EEPS compared to that of Khalek et al. for stoichiometric GDI [21].

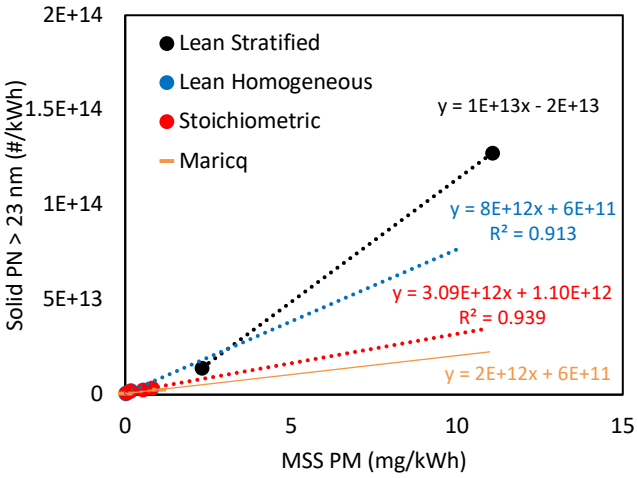

Figure 9. Correlation between SPN > 23 nm and soot emissions measured by MSS compared with the PN to PM reported by Maricq et al. for stoichiometric GDI [33].

Figure 10 summarizes the results of the transient conditions showing the characteristic temporal soot, PN, and PSD evolution over stoichiometric and lean homogeneous load steps as well as stoichiometric cold starts. Note that the soot scale is multiplied by a factor of 10 to display small variations in concentration. For all of these conditions, the transient event occurs at an elapsed time equal to approximately 60 seconds. Each transient condition was performed during three separate tests as with the steady state conditions, but the results are not averaged to not smooth out peaks that occurred on slightly different timescales from test to test. The magnitude of these events show good repeatability. The PN and soot spikes and final concentrations were consistent for all transients, however, the initial PN and soot concentration of the stoichiometric load step at 2000

rpm 2 bar BMEP had significant variation from test to test. The soot and PN concentration were approximately 0.2 +/- 0.2 mg/m^3 and 3.0 x 10^6 +/- 1.9 x 10^6 #/cm^3 respectively. The stoichiometric load steps showed a significant but short spike in soot and PN followed a decrease in soot and PN. The soot spiked by a factor of about three and PN spiked by an order of magnitude. The PN spike is dominated by ash mode particles. It is unusual that soot concentration would decrease with an increase in load. It is suspected that this engine has poor charge motion to retain fuel stratification at low speed and load where the factory calibration defaults to the lean stratified mode. Additionally, if the engine is left running at 2000 rpm 7 bar BMEP, the soot concentration was found to "creep" to its steady state concentration of approximately 0.2 mg/m^3 within 10 minutes.

The soot concentration remained nearly constant throughout the lean homogeneous load steps at about 0.1 mg/m^3 and there was a modest increase in PN concentration. The increase in PN can be attributed to a spike in the ash mode.

The bottom two plots of Figure 10 show particle emissions during the cold start. During the first 30 seconds the engine was static, from t = 30 to 60 seconds the engine was motored, and injection and firing commenced at t = 60 seconds. It is worth noting that during the motoring period, when the engine was not fueled, there was a spike in PN emissions. This is consistent with the findings that both GDI and diesel engines emit nanoparticles even when not fueled [35]. This occurs regularly under ordinary driving conditions such as engine braking and there is no combustion strategy that can mitigate these emissions. Other than utilizing camless variable valve technology to keep the exhaust valves closed during deceleration, GPFs would be the only obvious solution for removing these particles from GDI exhaust. The PN emissions once injection and firing commenced were significant. The PN concentrations after the cold starts remain above 10^7 #/cm^3 for over a minute. This concentration corresponds to an emission rate of approximately 3 x 10^{12} particles per minute. Again, these particles are almost entirely sub 23-nm. The presence of soot normally associated with cold starts is absent here due to the lack of fuel enrichment for this testing.

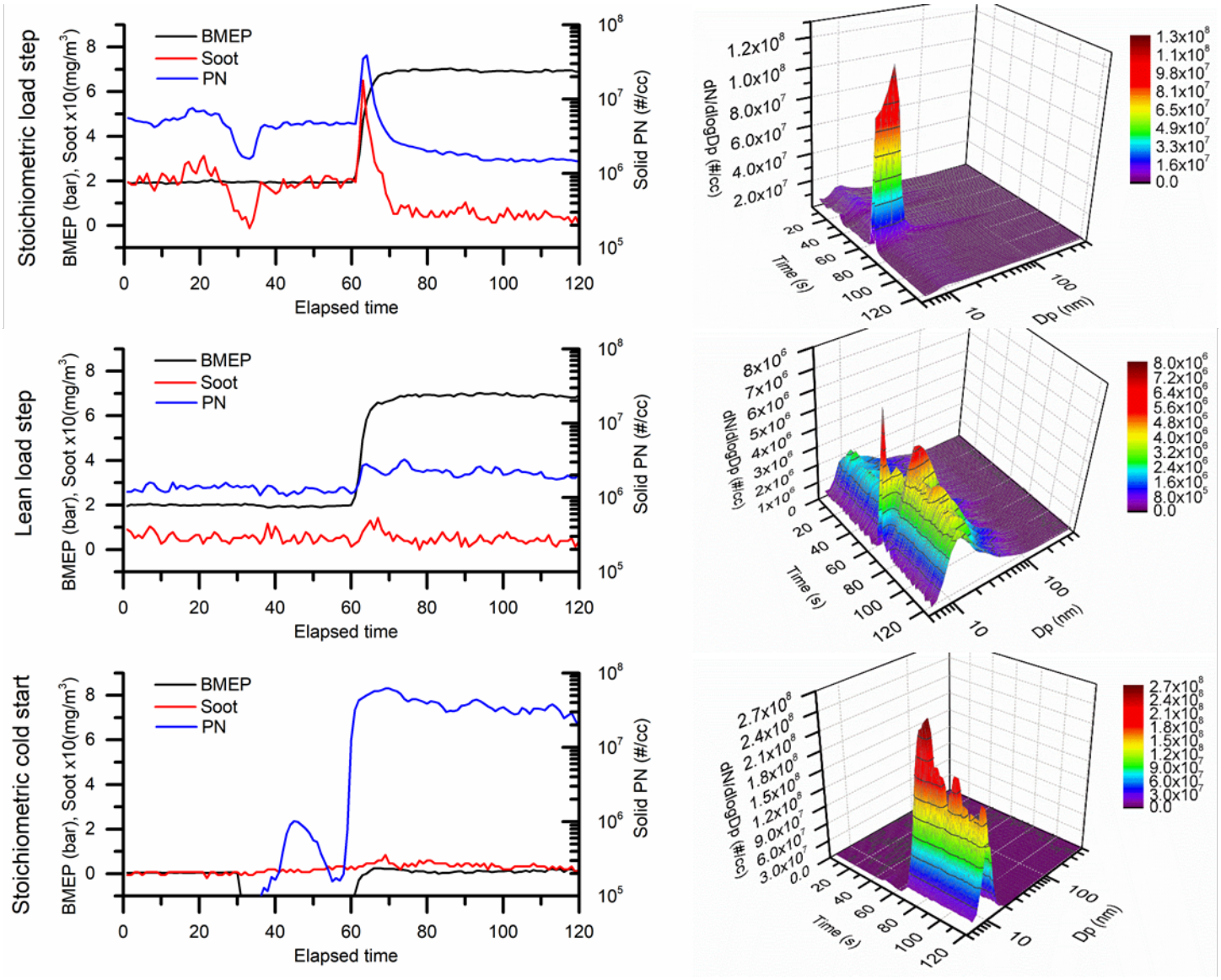

Figure 10. Soot, PN, and BMEP (left) and PSD (right) evolution over a stoichiometric constant speed load step (top), lean homogeneous constant speed load step (middle), and stoichiometric cold start (bottom).

Summary/Conclusion

Steady state and transient engine conditions have been evaluated for stoichiometric, lean homogeneous, and lean stratified operation in a GDI engine. The steady state lean stratified conditions produced an excessive amount soot and PM/PN emissions and only offered an efficiency advantage over lean homogeneous at very low load. The steady state stoichiometric conditions showed broad, flat particle size distributions which are unique compared to the traditional bimodal distribution commonly associated with engine combustion. The steady state lean homogeneous conditions showed favorable fuel efficiency across the operation range and relatively low PN and PM emissions, but a very high fraction of unregulated solid PN between 10 and 23 nm.

Stoichiometric PN to PM ratio were in good agreement to previous studies. However, both lean combustion modes showed higher particle number to mass ratios indicating more small particles per unit aerosol mass. The transient load steps and engine start showed minimal soot emissions but consistent spikes of ash mode PN. Stoichiometric engine cold starts emitted the highest concentration of PN besides the higher load lean stratified condition. The PN emissions from the engine cold start were almost entirely composed of sub-23 nm particles, thought to consist mostly of metallic ash derived from lubricating oil.

High ash particle concentrations found in all engine modes, but especially in lean homogeneous operation demonstrates that oil control is important for mitigating impacts on downstream gasoline particulate filters (GPF) from which ash particles are cannot be removed during filter regeneration. Because sub-23 nm particles are not regulated under current legislation, the high ash particle concentrations are of even greater concern if lean homogenous modes are to be employed in non-GPF equipped engines. The results of this study illustrate that ash particles need to be considered and better characterized in support of designing and operating lean GDI engines.

References

1. Alkidas, A.C. and Tahry, S.H. El, "Contributors to the Fuel Economy Advantage of DISI Engines Over PFI Engines," *SAE Tech. Pap.* 2003-01–31, 2003, doi:10.4271/2003-01-3101.
2. Liang, B., Ge, Y., Tan, J., Han, X., Gao, L., Hao, L., Ye, W., and Dai, P., "Comparison of PM emissions from a gasoline direct injected (GDI) vehicle and a port fuel injected (PFI) vehicle measured by electrical low pressure impactor (ELPI) with two fuels: Gasoline and M15 methanol gasoline," *J. Aerosol Sci.* 57:22–31, 2013, doi:10.1016/j.jaerosci.2012.11.008.
3. Saliba, G., Saleh, R., Zhao, Y., Presto, A.A., Lambe, A.T., Frodin, B., Sardar, S., Maldonado, H., Maddox, C., May, A.A., Drozd, G.T., Goldstein, A.H., Russell, L.M., Hagen, F., and Robinson, A.L., "Comparison of Gasoline Direct-Injection (GDI) and Port Fuel Injection (PFI) Vehicle Emissions: Emission Certification Standards, Cold-Start, Secondary Organic Aerosol Formation Potential, and Potential Climate Impacts," *Environ. Sci. Technol.* 51(11):6542–6552, 2017, doi:10.1021/acs.est.6b06509.
4. Maricq, M.M., Podsiadlik, D.H., and Chase, R.E., "Examination of the size-resolved and transient nature of motor vehicle particle emissions," *Environ. Sci. Technol.* 33(10):1618–1626, 1999, doi:10.1021/es9808806.
5. Szybist, J.P., Youngquist, A.D., Barone, T.L., Storey, J.M., Moore, W.R., Foster, M., and Confer, K., "Ethanol blends and engine operating strategy effects on light-duty spark-ignition engine particle emissions," *Energy and Fuels* 25(11):4977–4985, 2011, doi:10.1021/ef201127y.
6. Graskow, B. and Kittelson, D., "Exhaust Particulate Emissions from a Direct Injection Spark Ignition Engine," *SAE Tech. Pap.* 1999-01–11, 1999, doi:10.4271/1999-01-1145.
7. Chen, L., Liang, Z., Zhang, X., and Shuai, S., "Characterizing particulate matter emissions from GDI and PFI vehicles under transient and cold start conditions," *Fuel* 189:131–140, 2017, doi:10.1016/j.fuel.2016.10.0550016-2361.
8. Braisher, M., Stone, R., and Price, P., "Particle Number Emissions from a Range of European Vehicles," *SAE Int.*, 2010, doi:10.4271/2010-01-0786.
9. Zervas, E., Dorlhene, P., Daviau, R., and Dionnet, B., "Repeatability of fine particle measurement of diesel and gasoline vehicles exhaust gas," *SAE Tech.* 2004-01–19, 2004, doi:10.4271/2004-01-1983.
10. Mathis, U., Mohr, M., and Forss, A.M., "Comprehensive particle characterization of modern gasoline and diesel passenger cars at low ambient temperatures," *Atmos. Environ.* 39(1):107–117, 2005, doi:10.1016/j.atmosenv.2004.09.029.
11. Moore, W., Foster, M., Lai, M.-C., Xie, X.-B., Zheng, Y., and Matsumoto, A., "Charge Motion Benefits of Valve Deactivation to Reduce Fuel Consumption and Emissions in a GDi, VVA Engine," *SAE Tech. Pap.* 2011-01–12, 2011, doi:10.4271/2011-01-1221.
12. "LEV III" AMENDMENTS TO THE CALIFORNIA GREENHOUSE GAS AND CRITERIA POLLUTANT EXHAUST AND EVAPORATIVE EMISSION STANDARDS AND TEST PROCEDURES AND TO THE ON-BOARD DIAGNOSTIC SYSTEM REQUIREMENTS FOR PASSENGER CARS, LIGHT- DUTY TRUCKS, AND MEDIUM-DUTY VEHICLES, 1–161, 2012.
13. COMMISSION REGULATION (EU) No 459/2012, *Off. J. Eur. Union*, 2012.
14. Gidney, J.T., Twigg, M. V., and Kittelson, D.B., "Effect of organometallic fuel additives on nanoparticle emissions from a gasoline passenger car," *Environ. Sci. Technol.* 44(7):2562–2569, 2010, doi:10.1021/es901868c.
15. Mamakos, A., Martini, G., Marotta, A., and Manfredi, U., "Assessment of different technical options in reducing particle emissions from gasoline direct injection vehicles," *J. Aerosol Sci.* 63:115–125, 2013, doi:10.1016/j.jaerosci.2013.05.004.
16. Mayer, A.C., Ulrich, A., Czerwinski, J., and Mooney, J.J., "Metal-Oxide Particles in Combustion Engine Exhaust," *SAE Int.*, 2010, doi:10.4271/2010-01-0792.
17. Giechaskiel, B., Vanhanen, J., Väkevä, M., and Martini, G., "Investigation of vehicle exhaust sub-23 nm particle emissions," *Aerosol Sci. Technol.* 51:626–641, 2017, doi:10.1080/02786826.2017.1286291.
18. Kittelson, D.B., "Engines and nanoparticles: A review," *J. Aerosol Sci.* 29(5–6):575–588, 1998, doi:10.1016/S0021-

8502(97)10037-4.
19. Huang, Y.-W., Wu, C., and Aronstam, R.S., "Toxicity of Transition Metal Oxide Nanoparticles: Recent Insights from in vitro Studies," *Materials (Basel).* 3(10):4842–4859, 2010, doi:10.3390/ma3104842.
20. Oberdörster, G., Sharp, Z., Atudorei, V., Elder, A., Gelein, R., Kreyling, W., and Cox, C., "Translocation of inhaled ultrafine particles to the brain," *Inhal. Toxicol.* 16:437–445, 2004, doi:10.1080/08958370490439597.
21. Khalek, I.A., Bougher, T., and Jetter, J.J., "Particle Emissions from a 2009 Gasoline Direct Injection Engine Using Different Commercially Available Fuels," *SAE Int. J. Fuels Lubr.* 3(2):623–637, 2010, doi:10.4271/2010-01-2117.
22. Zhang, S. and McMahon, W., "Particulate Emissions for LEV II Light-Duty Gasoline Direct Injection Vehicles," *SAE Int. J. Fuels Lubr.* 5(2):2012-01–0442, 2012, doi:10.4271/2012-01-0442.
23. Peckham, M.S., Finch, A., Campbell, B., Price, P., and Davies, M.T., "Study of Particle Number Emissions from a Turbocharged Gasoline Direct Injection (GDI) Engine Including Data from a Fast-Response Particle Size Spectrometer," *SAE Int.* 2011-01–12, 2011, doi:10.4271/2011-01-1224.
24. Mayer, A., Czerwinski, J., Kasper, M., Ulrich, A., and Mooney, J.J., "Metal Oxide Particle Emissions from Diesel and Petrol Engines," *SAE Int.* 2012-01–08, 2012, doi:10.4271/2012-01-0841.
25. Giechaskiel, B., Manfredi, U., and Martini, G., "Engine Exhaust Solid Sub-23 nm Particles: I. Literature Survey," *SAE Int. J. Fuels Lubr.* 7(3):2014-01–2834, 2014, doi:10.4271/2014-01-2834.
26. Berndorfer, A., Breuer, S., Piock, W., and Bacho, P. Von, "Diffusion Combustion Phenomena in GDi Engines caused by Injection Process," *SAE Int.*, 2013, doi:10.4271/2013-01-0261.
27. Piock, W.F., Befrui, B., Berndorfer, A., and Hoffmann, G., "Fuel Pressure and Charge Motion Effects on GDi Engine Particulate Emissions," *SAE Int. J. Engines* 8(2):2015-01–0746, 2015, doi:10.4271/2015-01-0746.
28. Swanson, J. and Kittelson, D., "Evaluation of thermal denuder and catalytic stripper methods for solid particle measurements," *J. Aerosol Sci.* 41(12):1113–1122, 2010, doi:10.1016/j.jaerosci.2010.09.003.
29. Ntziachristos, L., Amanatidis, S., Samaras, Z., Giechaskiel, B., and Bergmann, A., "Use of a Catalytic Stripper as an Alternative to the Original PMP Measurement Protocol," *SAE Int. J. Fuels Lubr.* 6(2):532–541, 2013, doi:10.4271/2013-01-1563.
30. Apple, J., Gladis, D.D., Watts, W., and Kittelson, D., "Measuring Diesel Ash Emissions and Estimating Lube Oil Consumption Using a High Temperature Oxidation Method," *SAE Pap.* 2009-01–18, 2009, doi:10.4271/2009-01-1843.
31. Parks, J.E., Storey, J.M.E., Prikhodko, V.Y., Debusk, M.M., and Lewis, S.A., "Filter-Based Control of Particulate Matter from a Lean Gasoline Direct Injection Engine," *SAE 2016 World Congr. Exhib.* 12, 2016, doi:10.4271/2016-01-0937.
32. Zelenyuk, A., Wilson, J., Imre, D., Stewart, M., Muntean, G., Storey, J., Prikhodko, V., Lewis, S., Eibl, M., and Parks, J., "Detailed characterization of particulate matter emitted by lean-burn gasoline direct injection engine," *Int. J. Engine Res.* 18(5–6):560–572, 2017, doi:10.1177/1468087416675708.
33. Maricq, M.M., Szente, J., Loos, M., and Vogt, R., "Motor Vehicle PM Emissions Measurement at LEV III Levels," *SAE Int. J. Engines* 4(1):597–609, 2011, doi:10.4271/2011-01-0623.
34. Kirchner, U., Vogt, R., and Maricq, M., "Investigation of EURO-5 / 6 Level Particle Number Emissions of European Diesel Light Duty Vehicles," *Sae Pap. 2010-01-0789*, 2010, doi:10.4271/2010-01-0789.
35. Rönkkö, T., Pirjola, L., Ntziachristos, L., Heikkilä, J., Karjalainen, P., Hillamo, R., and Keskinen, J., "Vehicle engines produce exhaust nanoparticles even when not fueled," *Environ. Sci. Technol.* 48:2043–2050, 2014, doi:10.1021/es405687m.

Contact Information

William F. Northrop
612-625-6854
wnorthro@umn.edu

Acknowledgments

This material is based upon work supported by the Department of Energy, Office of Energy Efficiency and Renewable Energy (EERE), under Award Number DE-EE0007217.

Disclaimer